Determination of differential-cross-section moments from polarization-dependent product velocity distributions of photoinitiated bimolecular reactions

T. Peter Rakitzis, S. Alex Kandel, and Richard N. Zare
Department of Chemistry, Stanford University, Stanford, California 94305

(Received 7 July 1997; accepted 2 September 1997)

We describe procedures for the measurement of the differential-cross-section moments of the velocity distribution of the state-selected products of photoinitiated bimolecular reactions using resonance-enhanced multiphoton ionization (REMPI) detection and some form of laboratory velocity selection such as time-of-flight mass spectrometry. The relative ionization probability of a single product molecule is presented in the form $I=1+f(\Theta,\Phi,\theta_\epsilon,\theta_u,A_q^{(k)\mathrm{stf}})$, where the angles Θ, Φ, and θ_ϵ describe the orientation of the product's laboratory velocity with the photolysis and probe laser polarizations, θ_u is the product laboratory scattering angle, and the $A_q^{(k)\mathrm{stf}}$ are the stationary target frame (STF) differential-cross-section moments. The STF is a reference frame defined by the laboratory velocity and the scattering plane. From the ionization probability, I, we derive a method to measure all five parameters with $k\leqslant 2$, the differential cross section, $1/\sigma(d\sigma_{00}/d\Omega_r)$, and the four polarization parameters $A_1^{(1)\mathrm{stf}}$, $A_0^{(2)\mathrm{stf}}$, $A_1^{(2)\mathrm{stf}}$, and $A_2^{(2)\mathrm{stf}}$ [where the $A_q^{(k)\mathrm{stf}}$ are equal to the polarization-dependent differential cross sections normalized by the differential cross section, $(d\sigma_{kq}^{\mathrm{stf}}/d\Omega_r)/(d\sigma_{00}/d\Omega_r)$]. The five parameters can be determined using only one rotational branch and several experimental geometries. We present simulations that show the effects of product polarization on experimental signals, and we discuss the effectiveness and limitations of inverting the measured signals to the $A_q^{(k)\mathrm{stf}}$. © *1997 American Institute of Physics.* [S0021-9606(97)00246-8]

I. INTRODUCTION

Product rotational polarization in chemical reactions is a signature of the forces at the transition state. In the past three decades, measurements of product rotational polarization in the laboratory frame have been made with polarized laser beams and techniques using electric deflection.[1] The dynamically significant reference frames, however, are unlikely to be coincident with the laboratory frame. The transformation of polarization parameters from the laboratory frame to other reference frames depends strongly on the scattering angle (as well as the reaction kinematics and the experimental method). Thus, measurements of product polarization parameters that are insensitive to the scattering angle are averaged in a way that decreases the magnitude of the polarization parameters, which makes them difficult to interpret (except for kinematically favorable cases, such as reactions of the type $H+LH\rightarrow HH+L$). The complete description of product polarization must be obtained from scattering-angle-resolved experiments. These measurements can be achieved with crossed-molecular-beam experiments using laser detection. Such experiments are difficult, however, and have been performed in only a few instances. Moreover, product polarization parameters have not been reported in these experiments.

In recent years, several research groups have used the photoloc method (photoinitiated bimolecular reactions under bulb conditions with laser detection) to measure state-resolved and state-to-state differential cross sections.[2–13] The use of polarized laser detection allows the measurement of product polarization. The nature of the one-photon photoinitiation step sets the restriction that complete polarization information can be measured only for polarization parameters of rank $k\leqslant 2$.[1,14] Because polarization parameters of rank $k>2$ are rarely reported for reaction products, this limitation is not a major drawback. The relative simplicity of photoloc experiments has allowed several groups to measure product polarization as a function of scattering angle. Hall and co-workers[4] and Brouard and co-workers[5–7,15,16] have measured product Doppler profiles with laser-induced fluorescence (LIF) and have used the bipolar-moment formalism of Dixon[17] to measure scattering-angle-dependent product polarization. Orr-Ewing *et al.*[18] have used the polarization-parameter formalism coupled with REMPI detection and the core extraction technique to measure the laboratory $A_0^{(2)}$ moment versus scattering angle for the $Cl+CH_4$ ($\nu_3=1$) reaction. Aoiz *et al.*[19] have described methods to measure polarization-dependent differential cross sections using the bipolar-moment formalism and LIF; these methods have been used by Brouard *et al.*[20] to measure several polarization-dependent differential cross sections for the state-selected OH product from the $H+CO_2$ reaction. Shafer-Ray *et al.*[14] used the powerful polarization parameter formalism and introduced the stationary target frame to explain the polarization dependence of the velocity distribution of photoloc experiments through straightforward formulas. Recently, Miranda and Clary[21] have shown how the correlation of reagent and product velocities and rotational polarization is related to the scattering matrix from quantum scattering calculations.

Using the polarization parameter approach of Shafer-Ray *et al.*[14] we discuss procedures for inverting the five polarization parameters of rank $k \leqslant 2$ [the $1/\sigma(d\sigma_{00}/d\Omega_r)$, $A_1^{(1)\mathrm{stf}}$, $A_0^{(2)\mathrm{stf}}$, $A_1^{(2)\mathrm{stf}}$, and $A_2^{(2)\mathrm{stf}}$] from data generated from photoloc experiments using REMPI detection on a single rotational branch and various experimental geometries (the inversion of parameters with $k>2$ merely requires additional experimental geometries). The definitions of the polarization parameters, relevant reference frames and transformations, and the methodology for the generation of polarization-dependent basis functions are developed in Sec. II. In Sec. III, we discuss the various experimental geometries needed to invert the polarization parameters from the data. Finally, experimental simulations are presented in Sec. IV to illustrate the effects of product polarization on experimental signals and to demonstrate procedures for inverting the polarization parameters.

II. POLARIZATION-DEPENDENT BASIS SET GENERATION

A. Polarization-independent differential cross sections

Our methodology for the measurement of the scattering-angle-dependent polarization parameters, $A_q^{(k)\mathrm{stf}}$, is a natural extension of our methods for the measurement of polarization-independent differential cross sections, $1/\sigma(d\sigma_{00}/d\Omega_r)$. These methods are described extensively elsewhere,[9] but a brief description included here will aid the discussion of the measurement of product polarization.

Molecules of AX and BC are coexpanded supersonically into a vacuum and attain the same beam velocity, such that their relative translational energy can be neglected. These molecules are assumed to be internally cold. The reaction of $A+BC \rightarrow AB+C$ is initiated by the laser photolysis of AX, which produces nearly monoenergetic molecules of A with a narrow spread of speeds, which in turn ensures a narrow spread of collision energies for the reaction. The allowed speed range of the AB product in the laboratory ($v_{\min} \leqslant v_{AB}^{\mathrm{lab}} \leqslant v_{\max}$) is easily calculated using energy- and momentum-conservation laws.[10] A one-to-one mapping exists between the laboratory speed and scattering angle (for a known amount of internal energy in AB and C). Hence, the measurement of the speed distribution of AB (v,J) suffices to determine the state-resolved differential cross section.

The velocity distribution of v_{AB}^{lab} can be thought of as a series of spherical shells in velocity space, each of radius v_{AB}^{lab}, with a surface density that is cylindrically symmetric with respect to the photolysis polarization axis [Fig. 1(a)]. The one-dimensional projection of a shell can be obtained with Doppler spectroscopy or by ionizing the AB molecules and detecting them with a velocity-sensitive time-of-flight mass spectrometer; in the latter case, the core-extraction technique[9] can be implemented by rejecting off-axis velocities with a mask, which provides a direct measurement of v_{AB}^{lab} [Fig. 1(b)]. In our experiments, time-of-flight profiles are fit with the output of a Monte Carlo simulation, in which molecules of a fixed laboratory speed are generated with the appropriate spatial anisotropy, and their trajectories through the mass spectrometer are simulated to generate the time-of-flight profile. A number of these forms, representing the range of speeds allowed for v_{AB}^{lab}, are used as a basis set for the analysis of data from experiments.

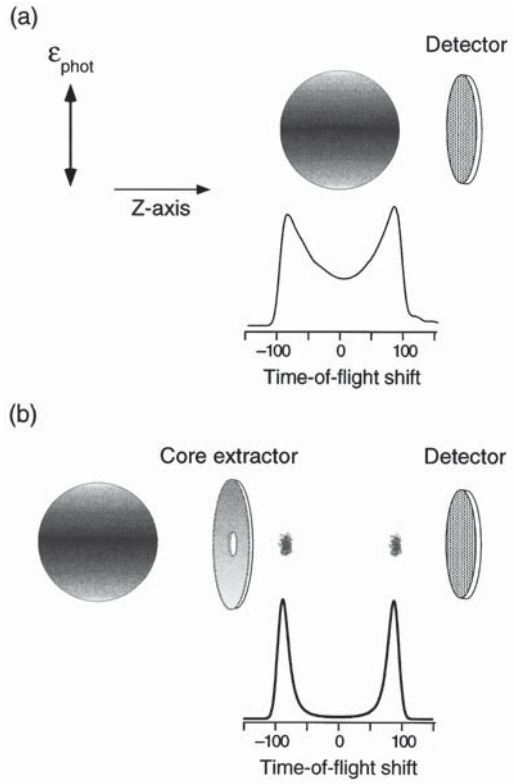

FIG. 1. (a) The ion-arrival profile for a monoenergetic speed distribution. (b) The ion-arrival profile using the core-extraction technique. The separation of the two peaks is proportional to the laboratory speed.

The basis set generation requires knowledge of the probability that an individual molecule is detected, P_{detect}, as a function of time of flight (or Doppler shift), given v_{AB}^{lab} and the spherical polar angles of v_{AB}^{lab} with respect to the detection axis (θ_{AB} and φ_{AB})

$$P_{\mathrm{detect}}(t) = f(v_{AB}^{\mathrm{lab}}, \theta_{AB}, \varphi_{AB}). \tag{1}$$

Hence, to include product polarization into the basis set generation procedure, we must merely include in the detection probability the ionization probability, I, as a function of the polarization parameters, $A_q^{(k)\mathrm{lab}}$, v_{AB}^{lab}, and the quantization axes of the photolysis and detection laser beams, $\boldsymbol{\epsilon}_{\mathrm{probe}}$ and $\boldsymbol{\epsilon}_{\mathrm{phot}}$

$$P_{\mathrm{detect}}(t) = f(v_{AB}^{\mathrm{lab}}, \theta_{AB}, \varphi_{AB}) \cdot I(A_q^{(k)\mathrm{lab}}, \boldsymbol{\epsilon}_{\mathrm{phot}}, \boldsymbol{\epsilon}_{\mathrm{probe}}, v_{AB}^{\mathrm{lab}}). \tag{2}$$

Before discussing the calculation of I, we turn our attention to the polarization parameters, $A_q^{(k)}$, the choice of reference frames, and how they are related.

B. Polarization parameters and reference frames

The rotational properties of an arbitrary ensemble of rotating molecules with angular momentum J can be completely described[1] by the $(2J+1)^2$ polarization parameters, $A_q^{(k)}$ ($k \leqslant 2J$ and $-k \leqslant q \leqslant k$), where

$$A_q^{(k)} = \frac{c(k)}{\langle JM|J^2|JM\rangle^{k/2}} \langle J_q^{(k)} \rangle, \tag{3}$$

and satisfy the relation

$$A_q^{(k)} = (-1)^q A_{-q}^{(k)*}. \tag{4}$$

Here, $J_q^{(k)}$ is the spherical-tensor angular momentum operator,[22] and $c(k)$ is a normalization constant.[1] The description of product rotational polarization from bimolecular reactions (from unpolarized reagents with an achiral reaction center) requires fewer parameters, however.[23] The use of the symmetry of the scattering plane gives the following relation for the $A_q^{(k)}$:

$$A_q^{(k)} = (-1)^{k+q} A_{-q}^{(k)}, \tag{5}$$

where the $A_q^{(k)}$ used here are defined with respect to a coordinate frame whose z axis is in the scattering plane; such coordinate frames include the experimentally convenient STF[14] and the physically significant RSF (reagent scattering frame) and PSF (product scattering frame). For the STF, $\hat{z}^{\rm stf}$ is parallel to $v_{AB}^{\rm lab}$, for the RSF, $\hat{z}^{\rm rsf}$ is parallel to u_A, whereas for the PSF, $\hat{z}^{\rm psf}$ is parallel to u_{AB}; in all three reference frames the y axis is perpendicular to the scattering plane. It follows from Eqs. (4) and (5) that the $A_q^{(k)}$ of even k are purely real and the $A_q^{(k)}$ of odd k are purely imaginary. Additionally, the symmetry of the scattering plane ensures that the parameters $A_0^{(k)}$ with odd k vanish. Hence, the number of polarization parameters necessary to describe the product rotational polarization from bimolecular reactions is reduced from $(2J+1)^2$ to $(2J^2+2J+1)$ for integral J and $(2J^2+2J+1/2)$ for half-integral J. In addition, as discussed in Sec. II C, the nature of the $(n+m)$ REMPI process limits the parameters that can be measured to those with $k \leqslant 2n$ (where it is assumed that the ionization step is saturated). For example, experiments employing the commonly used $(2+1)$ REMPI scheme are sensitive to parameters with $k \leqslant 4$ only.

The $A_q^{(k){\rm lab}}$ parameters are defined with respect to the $\hat{x}^{\rm lab}$, $\hat{y}^{\rm lab}$, and $\hat{z}^{\rm lab}$ axes in the laboratory frame [Fig. 2(a)]. Here, $\hat{z}^{\rm lab}$ is chosen to be parallel to $v_{AB}^{\rm lab}$, and $\hat{y}^{\rm lab}$ is perpendicular to the plane defined by $v_{AB}^{\rm lab}$ and $\epsilon_{\rm phot}$ ($\hat{y}^{\rm lab} = \hat{v}_{AB}^{\rm lab} \times \hat{\epsilon}_{\rm phot}$). A reference frame that is more dynamically significant than the laboratory frame is one that is defined with respect to the scattering plane of the $A+BC$ reaction. The stationary target frame, introduced by Shafer-Ray *et al.*,[14] is such a frame. The STF is the natural frame to describe product polarization from photoinitiated reactions, as it is the frame in which the fewest polarization parameters are needed to describe the experimental signals. The STF is closely related to the laboratory frame, as $\hat{z}^{\rm stf}$ is coincident with $\hat{z}^{\rm lab}$ and is also parallel with $v_{AB}^{\rm lab}$ [Fig. 2(b)]. However, $\hat{y}^{\rm stf}$ is perpendicular to the scattering plane defined by $v_{AB}^{\rm lab}$ and $v_A^{\rm lab}$ ($\hat{y}^{\rm stf} = \hat{v}_A^{\rm lab} \times \hat{v}_{AB}^{\rm lab}$). Hence, the laboratory frame and the STF

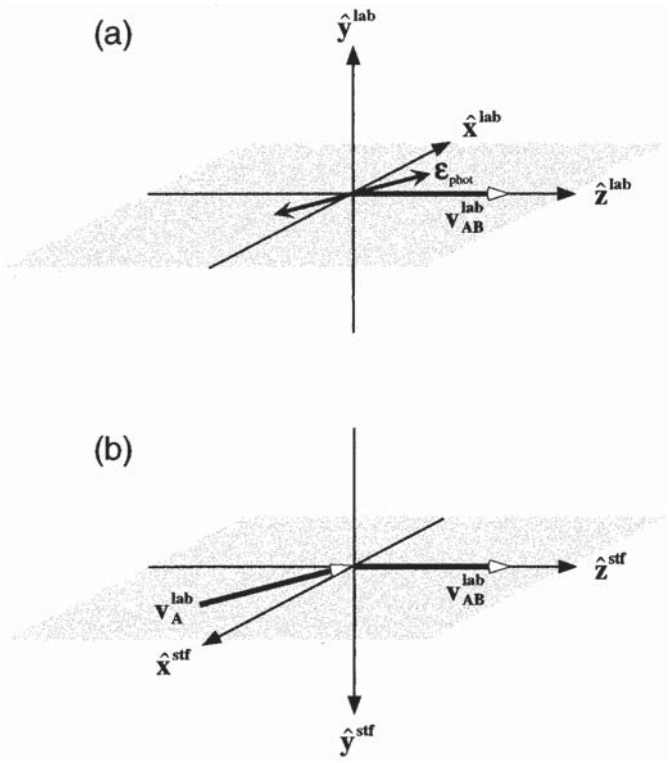

FIG. 2. (a) The laboratory frame. The $\hat{z}^{\rm lab}$ axis is parallel to $v_{AB}^{\rm lab}$, and $\hat{y}^{\rm lab}$ is perpendicular to the plane defined by $v_{AB}^{\rm lab}$ and the photolysis polarization axis, $\epsilon_{\rm phot}$. (b) The stationary target frame (STF). The $\hat{z}^{\rm stf}$ axis is also parallel to $v_{AB}^{\rm lab}$, whereas $\hat{y}^{\rm stf}$ is perpendicular to the scattering plane (defined by $v_{AB}^{\rm lab}$ and $v_A^{\rm lab}$). Note that when $\epsilon_{\rm phot}$ and $v_A^{\rm lab}$ are parallel, $\hat{y}^{\rm lab}$ and $\hat{y}^{\rm stf}$ are antiparallel (see text).

are simply related by a rotation about the $v_{AB}^{\rm lab}$ axis; this rotation is determined by the azimuthal angles of $v_A^{\rm lab}$ and $\epsilon_{\rm phot}$ about $v_{AB}^{\rm lab}$. A consequence of the definitions of the laboratory frame and the STF is that when $\epsilon_{\rm phot}$ and $v_A^{\rm lab}$ are parallel, $\hat{y}^{\rm lab}$ and $\hat{y}^{\rm stf}$ are antiparallel (Fig. 2). Defining the STF in this seemingly awkward fashion allows the STF to be transformed to the RSF through a single rotation using Wigner rotation matrices

$$A_q^{(k){\rm rsf}} = \sum_{q'=-k}^{k} D_{q'q}^k(0,-\theta_u,0) A_{q'}^{(k){\rm stf}}, \tag{6}$$

where θ_u is the laboratory scattering angle, given by $\cos\theta_u = \hat{u}_A \cdot \hat{v}_{AB}^{\rm lab}$, and $D_{qq'}^k(\varphi,\theta,\chi)$ is a Wigner rotation matrix.

We can express the $A_q^{(k){\rm lab}}$ in terms of the $A_q^{(k){\rm stf}}$

$$A_q^{(k){\rm lab}}(\chi) = \sum_{q'=-k}^{k} D_{q'q}^k(0,0,\chi-\pi) A_{q'}^{(k){\rm stf}}, \tag{7}$$

where χ is the relative azimuthal angle of $\epsilon_{\rm phot}$ and $v_A^{\rm lab}$ about $v_{AB}^{\rm lab}$; the phase difference of π ensures that $\hat{y}^{\rm stf}$ is parallel to $\hat{y}^{\rm rsf}$. Equation (7) can be expressed conveniently as

$$A_q^{(k){\rm lab}}(\chi) = (-1)^q e^{-iq\chi} A_q^{(k){\rm stf}}. \tag{8}$$

It is emphasized that Eqs. (7) and (8) refer to a single value of the azimuthal angle, χ. The explicit dependence of $A_q^{(k){\rm lab}}$ on χ will be removed by integrating over χ in Eq. (9).

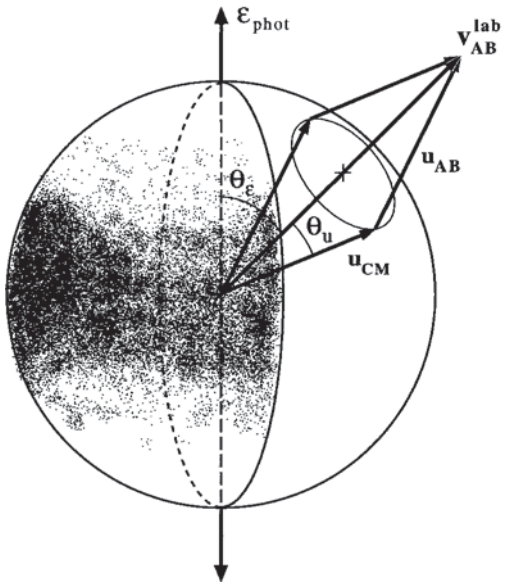

FIG. 3. The ensemble of products, AB, with laboratory velocity $v_{AB}^{\rm lab}$ are produced from an ensemble of reactants. A, whose velocities, $v_A^{\rm lab}$, form a cone of angle θ_u about $v_{AB}^{\rm lab}$. The density of the reactants as a function of the azimuthal angle about $v_{AB}^{\rm lab}$ depends on the angle between $v_{AB}^{\rm lab}$ and $\epsilon_{\rm phot}$, θ_ϵ, and $\beta_{\rm phot}$.

Product molecules, AB, with a particular velocity $v_{AB}^{\rm lab}$ (and hence with a particular laboratory scattering angle, θ_u) are produced from reactants, A, whose velocities, $v_A^{\rm lab}$, form a cone of angle θ_u about $v_{AB}^{\rm lab}$ (Fig. 3). As before, χ is the azimuthal angle of $v_A^{\rm lab}$ about $v_{AB}^{\rm lab}$ with respect to the plane defined by $v_{AB}^{\rm lab}$ and $\epsilon_{\rm phot}$. The $A_q^{(k){\rm lab}}$ for the ensemble of molecules AB with velocity $v_{AB}^{\rm lab}$ is the average of the $A_q^{(k){\rm lab}}(\chi)$ over all scattering events weighted by the density of reactant A, $D(\chi)$

$$A_q^{(k){\rm lab}}=\frac{\int_0^{2\pi}D(\chi)(-1)^q e^{-iq\chi}d\chi}{\int_0^{2\pi}D(\chi)d\chi}\,A_q^{(k){\rm stf}}, \tag{9}$$

where $D(\chi)=1+\beta_{\rm phot}P_2(\cos\delta)$, $\cos\delta=\cos\theta_\epsilon\cos\theta_u+\sin\theta_\epsilon\sin\theta_u\cos\chi$, and θ_ϵ is the angle between $v_{AB}^{\rm lab}$ and $\epsilon_{\rm phot}$. Evaluating Eq. (9) yields the relationships between the STF and laboratory frame polarization parameters for photoloc experiments

$$A_0^{(k){\rm lab}}=A_0^{(k){\rm stf}}, \tag{10}$$

$$A_1^{(k){\rm lab}}=\left(\frac{-3\beta_{\rm phot}\sin 2\theta_\epsilon\sin 2\theta_u}{8N(\theta_\epsilon,\theta_u)}\right)A_1^{(k){\rm stf}}, \tag{11}$$

$$A_2^{(k){\rm lab}}=\left(\frac{3\beta_{\rm phot}\sin^2\theta_\epsilon\sin^2\theta_u}{8N(\theta_\epsilon,\theta_u)}\right)A_2^{(k){\rm stf}}, \tag{12}$$

and

$$A_q^{(k){\rm lab}}=0 \quad \text{for } q>2 \tag{13}$$

where

$$N(\theta_\epsilon,\theta_u)=\frac{1}{2\pi}\int_0^{2\pi}D(\chi)d\chi$$
$$=1+\beta_{\rm phot}P_2(\cos\theta_\epsilon)P_2(\cos\theta_u). \tag{14}$$

Equation (13) shows why the STF is the natural frame to describe product polarization from photoinitiated reactions, as it is the frame in which the fewest linearly independent polarization parameters are needed to describe the experimental signals. In general, all $2k+1$ polarization parameters of a given k and reference frame are necessary to calculate alignment parameters of other reference frames, as shown by

$$A_q^{(k)\alpha}=\sum_{q'=-k}^{k}D^k_{q'q}(\varphi_{\alpha\beta},\theta_{\alpha\beta},\chi_{\alpha\beta})A_{q'}^{(k)\beta}, \tag{15}$$

where the Euler angles $\varphi_{\alpha\beta}$, $\theta_{\alpha\beta}$, and $\chi_{\alpha\beta}$ characterize the rotation between frames α and β. Thus, photoloc experiments are sensitive to this complete set of alignment parameters only for $k\leqslant 2$. Additionally, if θ_u is kinematically constrained to be small, then photoloc experiments lose sensitivity to the $A_2^{(k){\rm stf}}$ parameters proportionally to $\sin^2\theta_n$, and the $A_1^{(k){\rm stf}}$ parameters, proportionally to $\sin 2\theta_u$; in the limit of small θ_u, experiments are sensitive to the $A_0^{(k){\rm stf}}$ parameters only. Although only the $A_0^{(k){\rm stf}}$ can be measured in this limit, the STF becomes coincident with the physically significant reagent scattering frame, with $\hat{z}^{\rm stf}$ parallel to u_A.

As mentioned earlier, the $A_q^{(k){\rm stf}}$ are equivalent to the $(d\sigma_{kq}^{\rm stf}/d\Omega_r)/(d\sigma_{00}/d\Omega_r)$.[19] As such, the $A_q^{(k){\rm stf}}$ are a measure of the scattering-angle dependent product polarization, written explicitly as $A_q^{(k){\rm stf}}(\theta)$, where θ is the center-of-mass scattering angle; however, even though the polarization is described as a function of the center-of-mass scattering angle, the polarization itself is measured with respect to the stationary target frame (STF). The $A_q^{(k){\rm stf}}$ can then be rotated to any other frame as shown in Eq. (13). Notice that the term $d\sigma_{00}/d\Omega_r$, requires no superscript, as $d\sigma_{00}/d\Omega_r=d\sigma_{00}^{\rm stf}/d\Omega_r=d\sigma_{00}^{\rm rsf}/d\Omega_r$ since they are invariant upon rotation, and hence do not require the specification of a coordinate frame.

C. Product ionization probability

The relative ionization intensity of a molecule $AB(v,J)$ in a REMPI process with polarized light can be expressed in terms of the polarization parameters in a simple form[24,25]

$$I(\Theta,\Phi,A_q^{(k){\rm lab}})=\sum_{k=0}^{2n}\sum_{q=-k}^{k}\left(\frac{4\pi}{2k+1}\right)^{1/2}s_k Y_q^k(\Theta,\Phi)A_q^{(k){\rm lab}}, \tag{16}$$

where the ionization sensitivity, s_k, depends on the details of spectral transition of the resonant step, such as the quantum numbers of the ground state and the resonant state, J_i, Λ_i, J_f, and Λ_f. Methods for calculating the s_k for $2+1$ REMPI have been reported by Kummel *et al.*;[25,26] using the notation in these references, the s_k for linearly and circularly polarized probe light are given by

$$s_k=\frac{P_{0+}^{\{k\}}(J_i,J_f,\beta=0,\Delta)/G(k,q,\phi',\theta',\chi',\Delta)}{P_{0+}^{\{0\}}(J_i,J_f,\beta=0,\Delta)}$$

for linearly polarized light (17)

and

$$s_k=\frac{P_{0+}^{\{k\}}(J_i,J_f,\beta=45,\Delta)/G(k,q,\phi',\theta',\chi',\Delta)}{P_{0+}^{\{0\}}(J_i,J_f,\beta=45,\Delta)}$$

for circularly polarized light. (18)

The terms of Eq. (16) that depend on the experimental geometry are contained in the $Y_q^k(\Theta,\Phi)$, where Θ is the angle between the detection axis (in this case $v_{AB}^{\rm lab}$) and the polarization axis of the detection laser beam, $\epsilon_{\rm probe}$; Φ is the angle between the projections of $\epsilon_{\rm probe}$ and $\epsilon_{\rm phot}$ onto the plane perpendicular to the detection axis; and n is the number of photons in the resonant step of the $(n+m)$ REMPI process, of which the ionization step is assumed to be saturated.

The general expression of Eq. (16) for the ionization of a molecule in the laboratory frame can be combined with the frame transformations of Eqs. (10)–(12) to give a complete description of the ionization probability of the products of (one-photon) photoinitiated bimolecular reactions

$$I(\Theta,\Phi,\theta_\epsilon,\theta_u,A_q^{(k)\rm stf})=1+\sum_{k=1}^{2\pi}\left(\frac{4\pi}{2k+1}\right)^{1/2}s_k\left\{Y_0^k(\Theta,0)A_0^{(k)\rm stf}-\frac{3\beta_{\rm phot}}{8N(\theta_\epsilon,\theta_u)}\sin 2\theta_\epsilon\sin 2\theta_u[e^{i\Phi}+(-1)^k e^{-i\Phi}]Y_1^k(\Theta,0)A_1^{(k)\rm stf}\right.$$
$$\left.+\frac{3\beta_{\rm phot}}{8N(\theta_\epsilon,\theta_u)}\sin^2\theta_\epsilon\sin^2\theta_u[e^{2i\Phi}+(-1)^k e^{-2i\Phi}]Y_2^k(\Theta,0)A_2^{(k)\rm stf}\right\},\tag{19}$$

where the isotropic $A_0^{(0)}$ term is normalized to unity, and $N(\theta_\epsilon,\theta_u)$ is defined in Eq. (14). Note that the s_k and the $A_q^{(k)\rm stf}$ of even k are purely real and the $A_q^{(k)\rm stf}$ of odd k are purely imaginary; the k dependence of the exponential terms ensures that the ionization expression is always purely real. Equation (19) is the most important result of this paper. It gives the relative probability of ionization of a product molecule, AB, with laboratory velocity, $v_{AB}^{\rm lab}$, as a function of its orientation with respect to $\epsilon_{\rm probe}$ and $\epsilon_{\rm phot}$ (defined by the angles Θ, Φ, and θ_ϵ), the laboratory frame scattering angle, θ_u, and the fewest necessary polarization parameters, $A_q^{(k)\rm stf}$ (with $k\leqslant 2n$ and $0\leqslant q\leqslant 2$). In this form, Eq. (19) is used in the Monte Carlo generation of polarization-dependent basis functions [Eq. (2)]. For each product molecule in the Monte Carlo simulation, only the angles Θ, Φ, and θ_ϵ need to be calculated to determine the relative ionization probability.

The relationship between $v_{AB}^{\rm lab}$ and θ_u must be known for the construction of polarization-dependent basis functions. If the internal energy of the unobserved product, C, is known, this relationship is uniquely determined.[10] If the internal energy of C is not known, then a previous measurement of the AB product spatial anisotropy can be used to determine this relationship. An advantage of the core-extraction method is that it decouples the measurement of the spatial anisotropy from the measurement of product polarization. This feature allows the measurement of the product spatial anisotropy even if the rotational polarization effects are large.

For cases in which the number of polarization parameters is limited to those with $k\leqslant 2$ [such as when using (1+1) REMPI or detecting product with $J'=1$, as is the case in the companion paper], the general ionization expression of Eq. (19) can be simplified to

$$I(\Theta,\Phi,\theta_\epsilon,\theta_u,A_q^{(k)\rm stf})$$
$$=1+s_2P_2(\cos\Theta)A_0^{(2)\rm stf}$$
$$-2\frac{(3/8)^{3/2}\beta_{\rm phot}}{1+\beta_{\rm phot}P_2(\cos\theta_\epsilon)P_2(\cos\theta_u)}$$
$$\times\{s_1\sin 2\theta_\epsilon\sin 2\theta_u\sin\Theta\sin\Phi(iA_1^{(1)\rm stf})$$
$$+s_2[\sin 2\theta_\epsilon\sin 2\theta_u\sin 2\Theta\cos\Phi A_1^{(2)\rm stf}$$
$$-\sin^2\theta_\epsilon\sin^2\theta\sin^2\Theta\cos 2\Phi A_2^{(2)\rm stf}]\}.\tag{20}$$

D. Polarization-dependent basis functions

Ionization measurements using isotropic probe light are not sensitive to polarization parameters with $k>0$; also, photoloc experiments with an isotropic photolytic source are not sensitive to polarization parameters with $q>0$. The generated basis functions, $B_G^{F(i)}(kq)$, must satisfy these conditions (where an equally weighted sum of probe or photolysis polarizations along the X, Y, and Z axes gives isotropic light)

$$B_{\rm iso}^{F(i)}(00)=B_X^{F(i)}(kq)+B_Y^{F(i)}(kq)+B_Z^{F(i)}(kq)$$
$$(F=X,Y,Z)\tag{21}$$

and

$$B_G^{{\rm iso}(i)}(00)=B_G^{X(i)}(kq)+B_G^{Y(i)}(kq)+B_G^{Z(i)}(kq)$$
$$(G=X,Y,Z;q>0).\tag{22}$$

Here, the $B_G^{F(i)}(kq)$ are basis functions that exhibit a single $A_q^{(k)\rm stf}$ polarization parameter, in addition to the $A_0^{(0)\rm stf}$, which is proportional to the population, while F and G designate the laboratory orientation of $\epsilon_{\rm phot}$ and $\epsilon_{\rm probe}$, respectively. Hence, the basis function $B_G^{F(i)}(00)$ is independent of

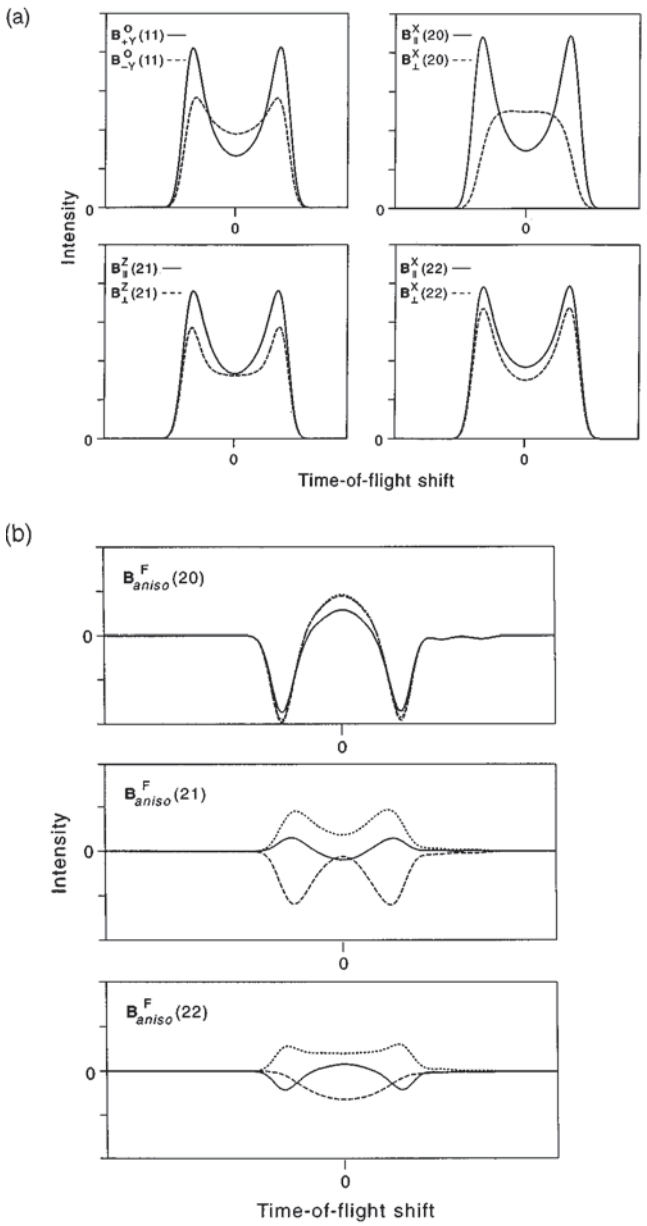

FIG. 4. Single speed core-extracted ion-arrival basis functions for the $Cl+C_2D_6$ reaction. (a) The effect of the geometry of the probe polarization on polarization-dependent basis functions. The basis functions are described with the $B^F_G(kq)$ notation; F indicates the geometry of $\epsilon_{\rm phot}$, and G indicates the geometry of $\epsilon_{\rm probe}$. (b) Single-speed anisotropic basis functions; the basis functions $B^{X(i)}_{\rm aniso}(2q)$, $B^{Y(i)}_{\rm aniso}(2q)$, and $B^{Z(i)}_{\rm aniso}(2q)$ are given by solid, dotted, and dashed lines, respectively.

polarization parameters with $k>0$. Equations (21) and (22) provide useful checks for the correctness of the basis-function generation procedure.

Figure 4(a) shows the dependence of the core-extracted basis functions that exhibit $A_1^{(1)\rm stf}$, $A_0^{(2)\rm stf}$, $A_1^{(2)\rm stf}$, and $A_2^{(2)\rm stf}$ polarization parameters on the geometry of the probe laser polarization. The experimental geometries used for these simulations are summarized in Table I, and the kinematics and energetics used to generate the basis functions are those for the $Cl+C_2D_6$ reaction, which is the subject of the companion paper.[27] The polarization parameters and the s_k in

TABLE I. The definition of laser polarization geometries. The angles θ_d and φ_d are the spherical polar angles about the detection axis.

Notation	θ_d	φ_d
X, $\perp$	90°	0°
Y	90°	90°
Z, $\parallel$	0°	0°
O	45°	90°

Fig. 4 have limiting values ($s_k=1$), and thus the polarization effects shown are also maximal. The limiting values for the $A_1^{(1)\rm stf}$, $A_0^{(2)\rm stf}$, $A_1^{(2)\rm stf}$, and $A_2^{(2)\rm stf}$ polarization parameters are shown in Table II. The basis functions in Fig. 4(a) represent the instrumental response to a single scattering angle, $\cos\theta=-0.37$, which corresponds to a laboratory scattering angle of $\theta_u=56°$. The parameters with $q=0$ are independent of θ_u, while those with $q=1$ are proportional to $\sin 2\theta_u$, and those with $q=2$ are proportional to $\sin^2\theta_u$. Therefore, at $\theta_u=56°$, the signals are sensitive to the $A_q^{(k)\rm stf}$ with $q\leqslant 2$. For the basis functions in Fig. 4(a), the position of the photolysis polarization was chosen to show maximal sensitivity for each $A_q^{(k)\rm stf}$. We notice that (for $k=2$) the basis functions are, for the chosen laser-polarization configurations, most sensitive to the $A_0^{(2)\rm stf}$ parameter, less sensitive to the $A_1^{(2)\rm stf}$ parameter, and least sensitive to the $A_2^{(2)\rm stf}$ parameter. This behavior is not a surprise. The experimental sensitivity to the speed-dependent polarization parameters depends on the speed resolution, the degree of velocity selection (through core extraction), the experimental laser polarization geometry and the reaction kinematics. In general, we expect the basis functions to be most sensitive to the $A_0^{(2)\rm stf}$ parameter (which is independent of θ_u and θ_ϵ), and least sensitive to the $A_2^{(2)\rm stf}$ parameter (which is proportional to $\sin^2\theta_\epsilon$ and $\sin^2\theta_u$).

Figure 4(b) shows probe-differenced anisotropic basis functions, $B^{F(i)}_{\rm aniso}(kq)$, given by $[B^{F(i)}_{\parallel}(kq)-B^{F(i)}_{\perp}(kq)]$, which are the difference between basis functions with the probe polarization parallel and perpendicular to the detection axis. In particular, we show how these probe-differenced basis functions transform as the photolysis polarization, $\epsilon_{\rm phot}$, is moved between the X, Y, and Z axes. The $B^{F(i)}_{\rm aniso}(20)$ basis functions barely change as the photolysis polarization is moved, because the $A_0^{(2)\rm stf}$ parameter does not depend explicitly on θ_ϵ (the small differences are caused by small changes in the spatial anisotropy and the slight breaking of cylindrical symmetry by the laser propagation directions). In contrast, the $B^{F(i)}_{\rm aniso}(21)$ and $B^{F(i)}_{\rm aniso}(22)$ basis functions depend strongly

TABLE II. Limiting values of the polarization parameters in the high J limit.

$A_q^{(k)}$	Minimum value	Maximum value
$A_1^{(1)}$	$-i/\sqrt{2}$	$+i/\sqrt{2}$
$A_0^{(2)}$	-1	$+2$
$A_1^{(2)}$	$-\sqrt{3/2}$	$+\sqrt{3/8}$
$A_2^{(2)}$	$-\sqrt{3/8}$	$+\sqrt{3/2}$

on the position of ϵ_{phot}. This variation allows us to separate their relative contributions.

III. MEASUREMENT OF THE POLARIZATION PARAMETERS

Using the polarization-dependent basis functions from Sec. II, we can use various approaches to extract the $A_q^{(k)\text{stf}}$ from experimental signals. Clearly, the number of independent experimental speed profiles that must be acquired is equal to the number of the $A_q^{(k)\text{stf}}$ to which the experiment is sensitive. These profiles can be obtained by detecting the product using different rotational branches or by using different laser-beam polarization geometries. The s_k from Eq. (19) depend on the rotational branch, and the angles Θ, Φ, and θ_ϵ in Eq. (19) depend on the laser polarization geometry. Brouard *et al.*[20] used three detection geometries and detected the product on two rotational branches; this method requires normalizing signals that come from fairly different experimental conditions. This technique is not feasible for our experiments, in which we measure very small polarization-dependent signals due to strong hyperfine depolarization effects. For this reason, we will describe an inversion procedure that compares experimental signals that differ only in the direction of the probe polarization. It is further assumed that the signals from these two geometries can be normalized to each other to an accuracy that is significantly greater than the expected differences. This normalization can be done easily using various techniques. For example, we alternate between the two geometries on a shot-to-shot basis using a photoelastic modulator. The advantage of this procedure is that the difference of these two profiles is proportional to the polarization parameters only and that the fitting of such difference profiles allows the direct inversion of the signals to yield the $A_q^{(k)\text{stf}}$.

In this section, we describe the measurement of the $A_q^{(k)\text{stf}}$ with $k \leqslant 2$, the $A_1^{(1)\text{stf}}$, $A_0^{(2)\text{stf}}$, $A_1^{(2)\text{stf}}$, and $A_2^{(2)\text{stf}}$. The measurement of $A_q^{(k)\text{stf}}$ with $k \geqslant 2$ is merely an extension of these procedures, requiring more detection geometries and experimental diligence. The measurement of polarization parameters with elliptically polarized light is discussed by Kummel *et al.* for $(2+n)$ REMPI.[26] We follow the convention that polarization parameters with even k are referred to as alignment parameters, and those with odd k as orientation parameters. Linearly polarized probe light is sensitive only to the alignment parameters, whereas circularly polarized light is sensitive to both. Although the use of elliptically polarized light has some advantages, for simplicity, we choose to describe separately the measurement of polarization parameters with even k (with linearly polarized probe light) and odd k (with circularly polarized probe light).

A. Measurement of alignment parameters

1. Kinematically constrained reactions

If θ_u is kinematically constrained to be small [as is true for the $Cl+CD_4$ reaction, shown in Fig. 5(a)], then the sensitivity to the $A_2^{(2)\text{stf}}$, proportional to $\sin^2\theta_u$, is reduced and can be neglected. The contribution from the $A_1^{(2)\text{stf}}$ (proportional to $\sin 2\theta_u$) cannot be ignored in general, but if ϵ_{phot} is perpendicular to the detection axis, then the sensitivity to the $A_1^{(2)\text{stf}}$ is also negligible. Therefore, in this experimental configuration, the $A_0^{(2)\text{stf}}$ is responsible for the bulk of the probe polarization effects. Thus, by varying the direction of the probe polarization we can determine the $A_0^{(2)\text{stf}}$. Only two different directions are needed. For example, consider the two experimental signals $I_\parallel^X$ and $I_\perp^X$ (defined in Table I). The X superscript denotes that ϵ_{phot} is aligned along the X axis; the subscripts denote that ϵ_{probe} is parallel ($\parallel$) and perpendicular ($\perp$) to the detection axis. We define composite profiles of experimental signals

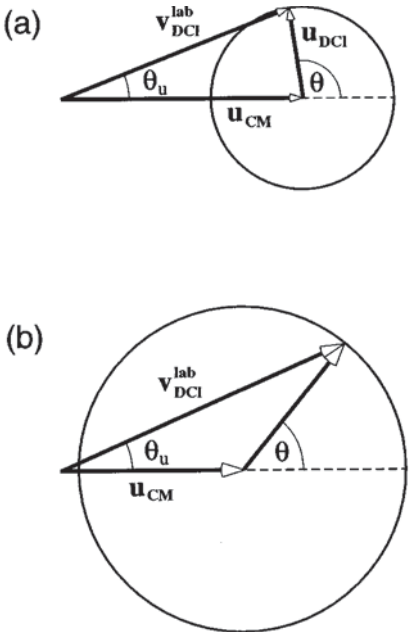

FIG. 5. Newton diagrams for (a) the $Cl+CD_4 \rightarrow DCl+CD_3$ reaction, for which the laboratory scattering angle, θ_u, is constrained to be always less than 20°; (b) the $Cl+C_2D_6 \rightarrow DCl+C_2D_5$ reaction, for which θ_u is not constrained to be small.

$$I_{\text{aniso}}^X = 2(I_\parallel^X - I_\perp^X) \tag{23}$$

and

$$I_{\text{iso}}^X = I_\parallel^X + 2I_\perp^X . \tag{24}$$

The composite time-of-flight profile I_{iso}^X is isotropic with respect to product polarization and is proportional to the differential cross section only. In contrast, the profile I_{aniso}^X is proportional to the $A_0^{(2)\text{stf}}$ and the differential cross section. The isotropic and anisotropic time-of-flight profiles can be expressed in terms of expansions of the appropriate basis functions

$$I_{\text{iso}}^Y = \sum_{i=1}^{N} c_{00}^{(i)} B_{\text{iso}}^{Y(i)}(20) \tag{25}$$

and

$$I_{\text{aniso}}^Y = \sum_{i=1}^{N} A_0^{(2)\text{stf}(i)} c_{00}^{(i)} B_{\text{aniso}}^{Y(i)}(20), \tag{26}$$

where the superscript i denotes a particular laboratory speed, and the N basis function speeds are equally spaced through the allowed range of laboratory speeds (typically $N \approx 10$). These linear combinations are solved using the methods described by Simpson *et al.*[9] Eq. (25) is solved first to give the speed distribution, $c_{00}^{(i)}$. The transformation of the speed distribution to the differential cross section is straightforward.[9,10] The values of the $c_{00}^{(i)}$ are then used in Eq. (26) from which the $A_0^{(2)\mathrm{stf}}$ versus product laboratory speed is obtained directly.

2. General case

In the previous special case, the $A_0^{(2)\mathrm{stf}}$ can be determined with ϵ_{phot} fixed. For the $Cl+C_2D_6$ reaction, however, θ_u is not constrained to be small, as is shown by the Newton diagram in Fig. 5(b). For this reaction, and in general, three orthogonal photolysis geometries are necessary to measure the three $A_0^{(2)\mathrm{stf}}$, $A_1^{(2)\mathrm{stf}}$, and $A_2^{(2)\mathrm{stf}}$ laboratory-speed-dependent parameters. These geometries are used to obtain the time-of-flight difference profiles I_{aniso}^X, I_{aniso}^Y, and I_{aniso}^Z (Table I). If the polarization effects are small, then the isotropic profile can be approximated by

$$I_{\mathrm{iso}}^F = I_{\parallel}^F + 2I_{\perp}^F \quad (F=X,Y,Z). \tag{27}$$

If the polarization effects are large, the three photolysis polarization geometries must be normalized to each other, and the true isotropic profile is given by the average of the three normalized isotropic profiles

$$I_{\mathrm{iso}}^{\mathrm{iso}} = \tfrac{1}{3}(I_{\mathrm{iso}}^X + I_{\mathrm{iso}}^Y + I_{\mathrm{iso}}^Z). \tag{28}$$

If the polarization effects are small, then the three unnormalized speed distributions, $c_{00}^{F(i)}$ (where $F=X,Y,Z$), will be the same within multiplicative constants. The three $c_{00}^{F(i)}$ distributions are easily obtained by fitting the three isotropic profiles with the appropriate basis function expansion:

$$I_{\mathrm{iso}}^F = \sum_{i=1}^{N} c_{00}^{F(i)} B_{\mathrm{iso}}^{F(i)}(20) \quad (F=X,Y,Z). \tag{29}$$

The three anisotropic profiles, I_{aniso}^X, I_{aniso}^Y, and I_{aniso}^Z, contain all the information necessary to obtain the three scattering-angle-dependent polarization parameters of rank $k=2$, the $A_0^{(2)\mathrm{stf}}$, $A_1^{(2)\mathrm{stf}}$, and $A_2^{(2)\mathrm{stf}}$. This task is accomplished, as shown in Eq. (30), by fitting all three anisotropic profiles simultaneously

$$I_{\mathrm{aniso}}^F = \sum_{i=1}^{N} \sum_{q=0}^{2} A_q^{(2)\mathrm{stf}(i)} c_{00}^{F(i)} B_{\mathrm{aniso}}^{F(i)}(2q) \quad (F=X,Y,Z). \tag{30}$$

If the effects of the polarization on the experimental signal are small, the I_{aniso}^X, I_{aniso}^Y, and I_{aniso}^Z profiles need not be normalized to each other; each I_{aniso}^F profile must be normalized with each I_{iso}^F profile, and this is done implicity by the $c_{00}^{F(i)}$ in Eq. (30). Thus, although experimental profiles must be acquired for six geometries (one of them redundant), the analysis of small experimental polarization effects requires the normalization between pairs of signals distinguished by the position of the probe polarization only; as mentioned earlier, this procedure is experimentally simple and can be done with great accuracy. If the experimental polarization effects are large, a true isotropic speed distribution must be obtained by fitting the true isotropic profile, shown in Eq. (28). This fitting will give

$$c_{00}^{\mathrm{iso}(i)} = c_{00}^{X(i)} = c_{00}^{Y(i)} = c_{00}^{Z(i)}, \tag{31}$$

and Eq. (30) can be inverted as before to give the $A_0^{(2)\mathrm{stf}}$, $A_1^{(2)\mathrm{stf}}$, and $A_2^{(2)\mathrm{stf}}$ parameters.

B. Measurement of orientation parameters

Our discussion of the measurement of orientation parameters is limited to the use of circularly polarized light. Circularly polarized light can be generated by passing linearly polarized light through a quarter waveplate. Right and left circularly polarized light is produced when the angle between the linear polarization of the probe light and the optical axis of the quarter wave plate, β, is equal to $\pm 45°$; for right circularly polarized light, the probe polarization, $\epsilon_{\mathrm{probe}}$, is parallel to the probe laser beam propagation direction, whereas for left circularly polarized light, $\epsilon_{\mathrm{probe}}$ is antiparallel to the probe laser beam propagation direction.

The ionization probabilities of left and right circularly polarized light are equally sensitive to alignment parameters. Therefore, the difference between time-of-flight profiles generated with left and right circularly polarized light are sensitive to the orientation parameters only (in this case, the $A_1^{(1)\mathrm{stf}}$):

$$I_{\mathrm{aniso}}^O = I_{+Y}^O - I_{-Y}^O, \tag{32}$$

where the $+Y$ subscript indicates that the probe polarization is oriented parallel to the Y axis, and $-Y$ indicates that $\epsilon_{\mathrm{probe}}$ is oriented antiparallel to the Y axis. The sensitivity to the $A_1^{(1)\mathrm{stf}}$ is maximized when the probe propagation direction, $\epsilon_{\mathrm{probe}}$, (along the Y axis) is perpendicular to the detection axis, and the photolysis polarization, ϵ_{phot}, is parallel to the O axis, which is 45° to the detection axis in the Y-Z plane (see Table I). In particular, the detection of the $A_1^{(1)\mathrm{stf}}$ requires that the photolysis polarization break the reflection symmetry of the plane defined by $\epsilon_{\mathrm{probe}}$ and the detection axis.

On the other hand, right and left circularly polarized light have equal but opposite sensitivity to orientation parameters. Thus, the sum of profiles generated with right and left circularly polarized light are independent of orientation parameters. This sum, however, is not independent of the alignment parameters, and it approximates the true isotropic profile only if the contributions of the alignment parameters to the signals are small

$$I_{\mathrm{iso}}^O = I_{+Y}^O + I_{-Y}^O. \tag{33}$$

We take advantage of this approximation in the companion paper and report the measurement of the $A_1^{(1)\mathrm{stf}}$ for the DCl ($v'=0$, $J'=1$) product from the $Cl+C_2D_6$ reaction.

If the contributions of the alignment parameters to the signals are large, the I_{iso}^0 profile can be simulated with

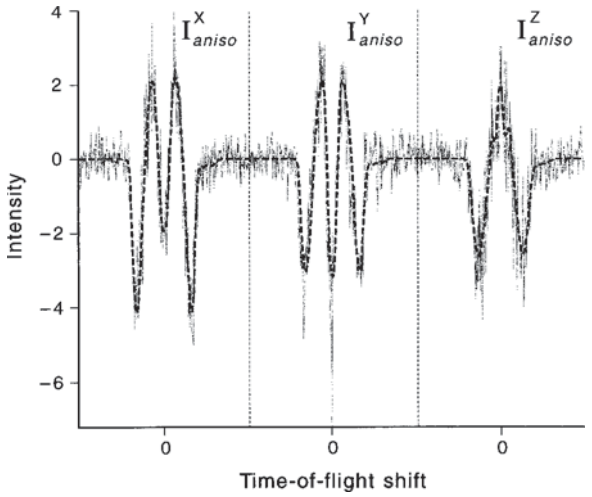

FIG. 6. Simulated product anisotropy signals I^X_{aniso}, I^Y_{aniso}, and I^Z_{aniso} along with the calculated best fit function. The solid line shows the simultaneous fit to all three profiles as a sum of instrumental basis functions obtained through a least-squares fitting algorithm.

knowledge of the $c_{00}^{(i)}$, $A_0^{(2)\text{stf}(i)}$, $A_1^{(2)\text{stf}(i)}$, and $A_2^{(2)\text{stf}(i)}$ from the alignment parameter measurements described in Sec. III A. The simulated profile and the experimental profile can be scaled to give the appropriate scaling factor, k, for the $c_{00}^{(i)}$:

$$I^O_{\text{iso}} = k \sum_{i=1}^{N} \sum_{q=0}^{2} A_q^{(2)\text{stf}(i)} c_{00}^{(i)} B^{O(i)}_{\text{iso}}(2q). \tag{34}$$

As before, the anisotropic profile can be expressed in terms of the appropriate basis function expansion

$$I^O_{\text{aniso}} = k \sum_{i=1}^{N} A_1^{(1)\text{stf}(i)} c_{00}^{(i)} B^{O(i)}_{\text{aniso}}(11). \tag{35}$$

Solution of Eq. (35) gives the $A_1^{(1)\text{stf}(i)}$.

IV. SIMULATIONS

In this section, we present simulated polarization data for the $Cl+C_2D_6 \rightarrow C_2D_5+DCl$ ($v'=0$, $J'=1$) reaction (which is the subject of the following paper). Our purpose is to illustrate typical polarization effects and to show the effectiveness and limitations of our inversion procedures using simulated data containing noise. We simulate constant polarization-dependent differential cross sections in the product scattering frame of $1/\sigma(d\sigma_{00}/d\Omega_r)=1.0$, $A_0^{(2)\text{psf}}=-1.0$, $A_1^{(2)\text{psf}}=0$, and $A_2^{(2)\text{psf}}=0$. The anisotropic profiles, I^X_{aniso}, I^Y_{aniso}, and I^Z_{aniso} are shown in Fig. 6; the signal-to-noise ratio shown here is approximately 5:1. These signals are fit with the methods described previously, and the resulting STF polarization-dependent differential cross sections are shown in Fig. 7, along with the cross sections from which the signals were generated. The error bars represent 2σ confidence intervals calculated from the 15-dimensional covariance ellipsoid from the nonlinear-least-squares fitting procedure. For simulations with no noise (not shown here), the $A_q^{(2)\text{stf}(i)}$ can be inverted exactly. As the noise in the simulations is increased, the error bars (which arise from the sensitivity and covariance of the basis functions relative to the signal-to-noise ratio) also increase. For the simulations shown in Fig. 6, we have chosen the magnitude of the signal-to-noise ratio so as to emphasize the relative sensitivity of the $A_q^{(2)\text{stf}(i)}$. In accord with our expectations from the discussion of basis function sensitivity in Sec. II D, we see from Fig. 7 that the analysis has the greatest sensitivity to the $A_0^{(2)\text{stf}}$ parameter, is less sensitive to the $A_1^{(2)\text{stf}}$ parameter, and is least sensitive to the $A_2^{(2)\text{stf}}$ parameter. The sensitivity to the $A_2^{(2)\text{stf}}$ parameter (proportional to $\sin^2\theta_u$) decreases in the forward scattered region as the laboratory scattering angle, θ_u, tends to zero, and the error bars show this effect. For the completely back-scattered product, the laboratory velocity, v^{lab}_{AB}, is nearly equal to zero. This virtually complete loss of velocity resolution causes the $A_0^{(2)\text{stf}}$, $A_1^{(2)\text{stf}}$ and $A_2^{(2)\text{stf}}$ parameters to become nearly linearly dependent in this region. This large covariance between the basis functions results in very large confidence limits for the back-scattered $A_q^{(2)\text{stf}(i)}$. In summary, for the noise levels used in this simulation, the $A_0^{(2)\text{stf}}$ can be measured very accurately, the $A_1^{(2)\text{stf}}$ can be measured less accurately, and the $A_2^{(2)\text{stf}}$ can be measured only qualitatively.

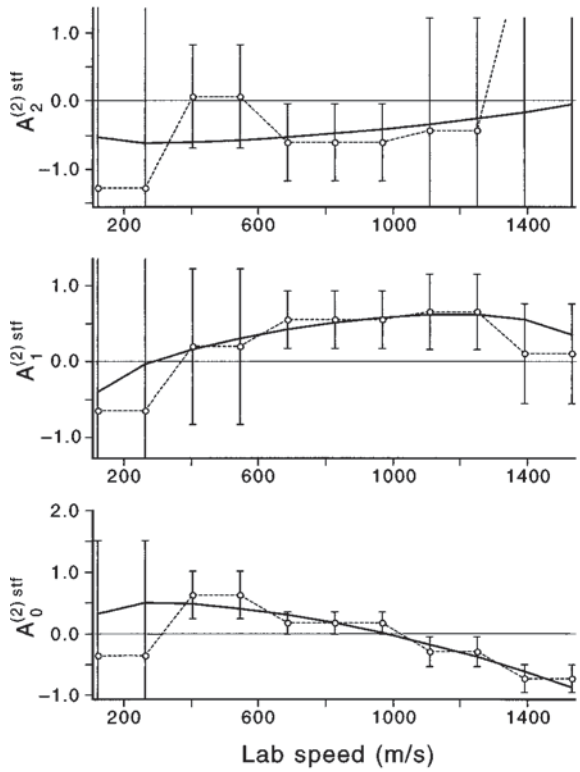

FIG. 7. Plots of the stationary target frame $A_0^{(2)\text{stf}}$, $A_1^{(2)\text{stf}}$, and $A_2^{(2)\text{stf}}$ scattering-angle-dependent polarization parameters resulting from analysis of the anisotropic time profiles shown in Fig. 6. The error bars represent 2σ confidence intervals calculated from the 15-dimensional covariance ellipsoid from the nonlinear-least-squares fitting procedure. The solid lines are the polarization parameters from which the simulated data in Fig. 6 were generated.

These simulations show that, for a particular scattering angle, the $A_0^{(2)\text{stf}}$ parameter can be measured very accurately,

whereas the uncertainty in the measurement of the $A_2^{(2)\mathrm{stf}}$ parameter can be larger than the physical range. This behavior demonstrates why the STF is the best frame to describe product polarization from photoloc experiments, as it is the frame in which the covariance of the $A_q^{(k)}$ is minimized. Once the experimental data has been analyzed in the STF, the $A_q^{(k)\mathrm{stf}}$ can be rotated to dynamically significant reference frames such as the RSF or PSF. In the companion paper, we apply the methods described here to measure the polarization of the DCI ($v'=0$, $J'=1$) product from the $Cl+C_2D_6$ and $Cl+CD_4$ reactions. In these experiments, the signal-to-noise ratio for the anisotropic signals is greater than 10:1, allowing a more accurate determination of the $A_q^{(2)\mathrm{stf}}$ than shown in the simulation.

ACKNOWLEDGMENTS

S.A.K. thanks the National Science Foundation for a predoctoral fellowship. We thank A. J. Orr-Ewing for useful discussions. This work has been supported by the National Science Foundation under grant No. CHE-93-22690.

[1] A. J. Orr-Ewing and R. N. Zare, Annu. Rev. Phys. Chem. **45**, 315 (1994).
[2] W. R. Simpson, T. P. Rakitzis, S. A. Kandel, A. J. Orr-Ewing, and R. N. Zare, J. Chem. Phys. **103**, 7313 (1995).
[3] G. E. Hall, in Proceedings of the Twelfth Combustion Research Conference, Livermore, CA, 1990 (The Combustion Research Facility of Sandia National Laboratory), p. 122.
[4] H. L. Kim, M. A. Wickramaaratchi, X. Zheng, and G. E. Hall, J. Chem. Phys. **101**, 2033 (1994).
[5] M. Brouard, S. P. Duxon, P. A. Enriquez, and J. P. Simons, J. Chem. Phys. **97**, 7414 (1992).
[6] M. Brouard, S. P. Duxon, P. A. Enriquez, and J. P. Simons, J. Chem. Soc. Faraday Trans. **89**, 1435 (1993).
[7] M. Brouard, S. P. Duxon, and J. P. Simons, Isr. J. Chem. **34**, 67 (1994).
[8] F. J. Aoiz, M. Brouard, P. A. Enriquez, and R. J. Sayos, J. Chem. Soc. Faraday Trans. **89**, 1427 (1993).
[9] W. R. Simpson, A. J. Orr-Ewing, S. A. Kandel, T. P. Rakitzis, and R. N. Zare, J. Chem. Phys. **103**, 7299 (1995).
[10] N. E. Shafer, A. J. Orr-Ewing, W. R. Simpson, H. Xu, and R. N. Zare, Chem. Phys. Lett. **212**, 155 (1993).
[11] H. Xu, N. E. Shafer-Ray, F. Merkt, D. J. Hughes, M. Springer, R. P. Tuckett, and R. N. Zare, J. Chem. Phys. **103**, 5157 (1995).
[12] D. F. Varley and P. J. Dagdigian, J. Phys. Chem. **100**, 4365 (1995).
[13] S. A. Kandel, T. P. Rakitzis, T. Lev-On, and R. N. Zare, J. Chem. Phys. **105**, 7550 (1996).
[14] N. E. Shafer-Ray, A. J. Orr-Ewing, and R. N. Zare, J. Phys. Chem. **99**, 7591 (1995).
[15] M. Brouard, S. P. Duxon, P. A. Enriquez, R. Sayos, and J. P. Simons, J. Phys. Chem. **95**, 8169 (1991).
[16] M. Brouard, M. T. Martinez, J. O'Mahony, and J. P. Simons, Mol. Phys. **69**, 65 (1990).
[17] R. N. Dixon, J. Chem. Phys. **85**, 1866 (1986).
[18] A. J. Orr-Ewing, W. R. Simpson, T. P. Rakitzis, S. A. Kandel, and R. N. Zare, J. Chem. Phys. **106**, 5961 (1997).
[19] F. J. Aoiz, M. Brouard, and P. A. Enriquez, J. Chem. Phys. **105**, 4964 (1996).
[20] M. Brouard, H. M. Lambert, S. P. Rayner, and J. P. Simons, Mol. Phys. **89**, 403 (1996).
[21] M. P. de Miranda and D. C. Clary, J. Chem. Phys. **106**, 4509 (1997).
[22] R. N. Zare, *Angular Momentum, Understanding Spatial Aspects in Chemistry and Physics* (Wiley, New York, 1988).
[23] K. Blum, *Density Matrix Theory and Applications* (Plenum, New York and London, 1981).
[24] D. A. Case, G. M. McClelland, and D. R. Herschbach, Mol. Phys. **35**, 541 (1978).
[25] A. C. Kummel, G. O. Sitz, and R. N. Zare, J. Chem. Phys. **85**, 6874 (1986).
[26] A. C. Kummel, G. O. Sitz, and R. N. Zare, J. Chem. Phys. **88**, 6707 (1988).
[27] T. P. Rakitzis, S. A. Kandel, T. Lev-On, and R. N. Zare J. Chem. Phys. **107**, 9392 (1997), following paper.